SUPPLEMENTARY MATERIAL

Zone determination – EMPA and NaOCl etch comparison

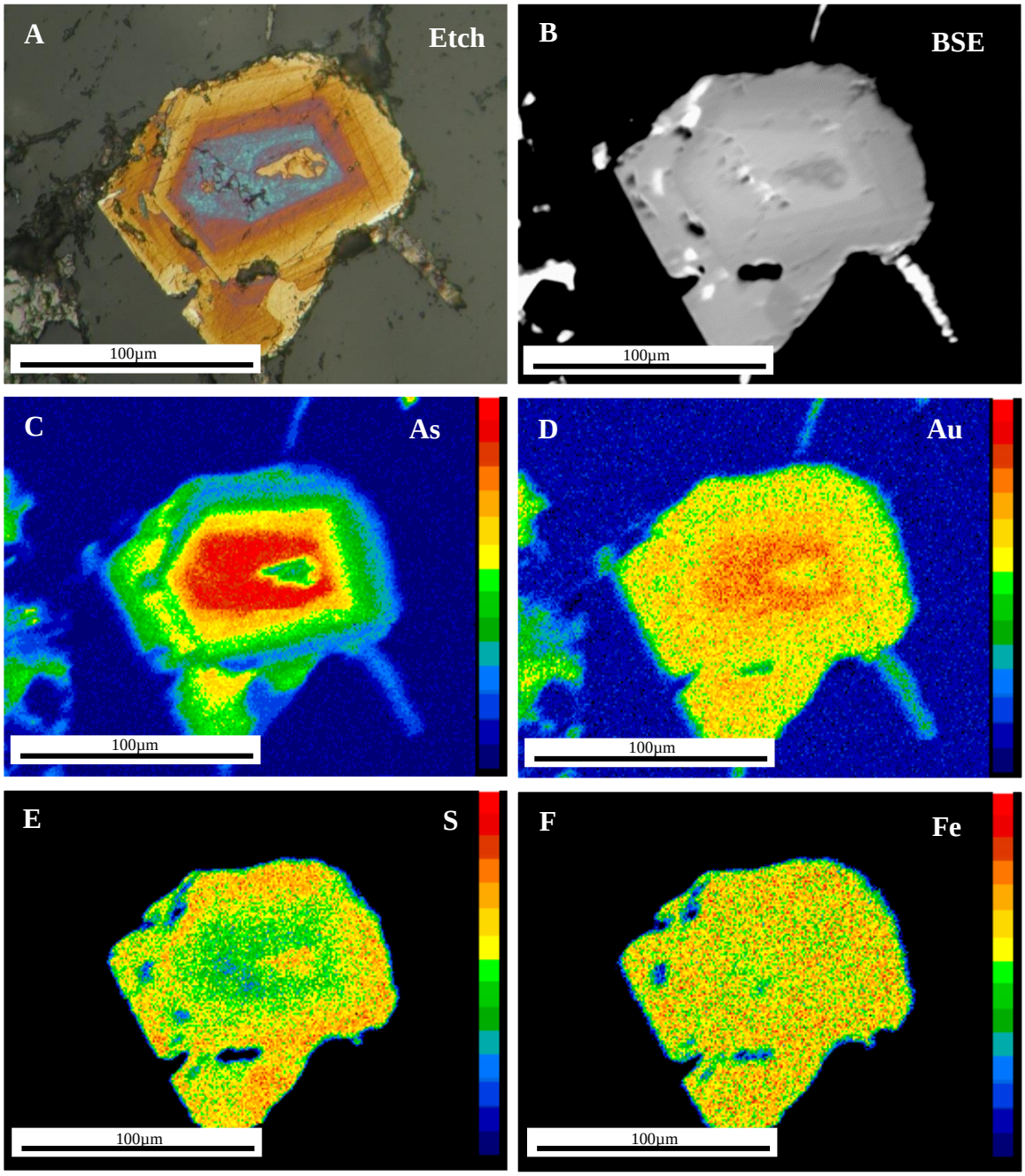

Figure DR1: Zoned pyrite crystal (PGC-214b.1) - (A) Reflected light photomicrograph of pyrite etched with NaOCl (B) Backscatter electron image. EMP element maps of (C) Arsenic, (D) Gold, (E) Sulfur and (F) Iron. Warm colours in (A) indicate greater trace element abundance. Cu EMP element map (not pictured) is similar to maps for Au and As.

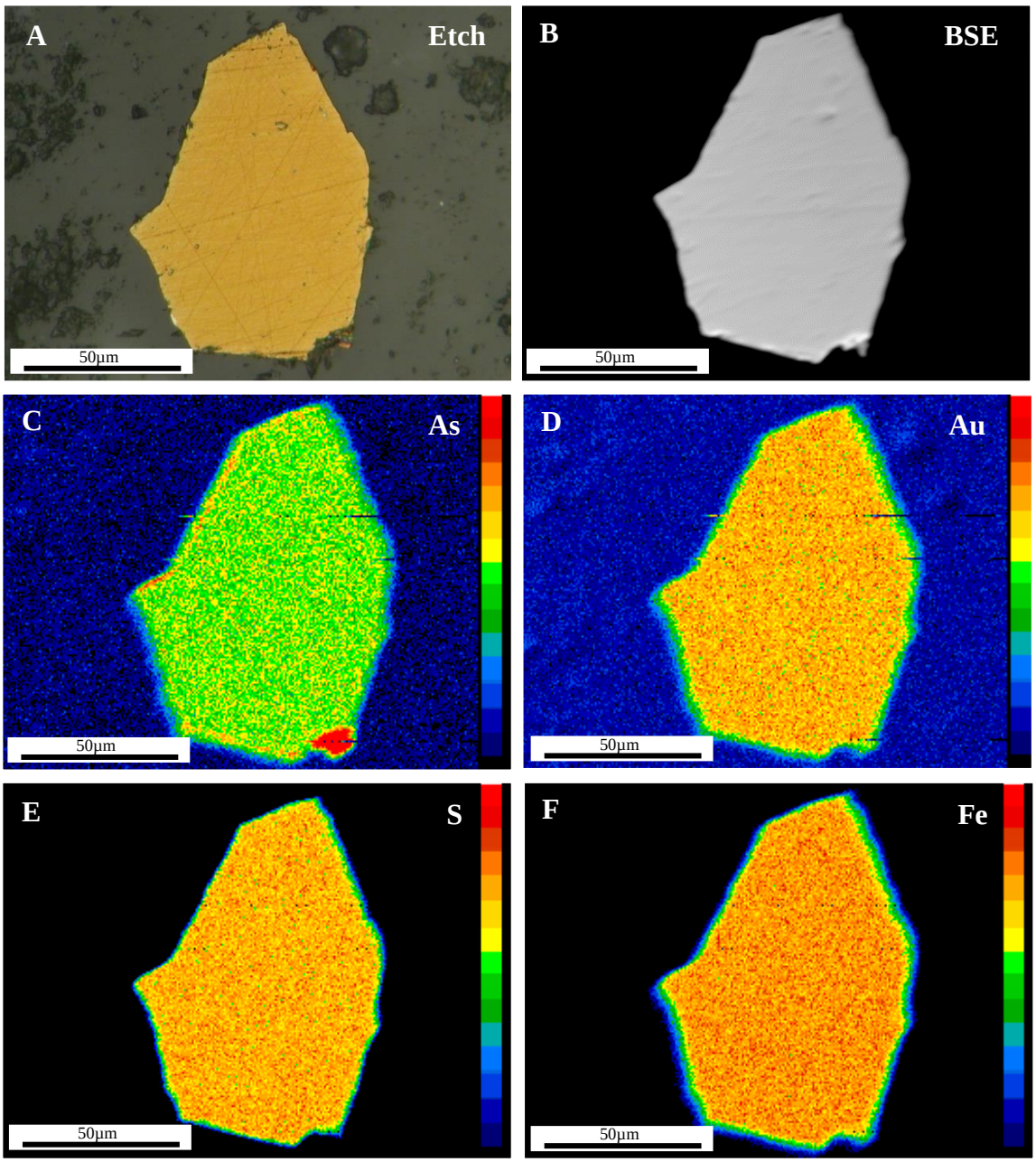

Figure DR2: Homogeneous pyrite crystal (PGC-214b.4) - (A) Reflected light photomicrograph of pyrite etched with NaOCl (B) Backscatter electron image. EMP element maps of (C) Arsenic, (D) Gold, (E) Sulfur and (F) Iron. Warm colours indicate greater element abundance. Cu EMP element map (not pictured) is similar to maps for Au and As.

Analytical Methods

Samples and sample preparation

A comprehensive suite of Porgera mine samples (well-documented for location, depth, structural setting, paragenesis etc.) was collected by Greg Cameron and Stuart Munroe between 1994 and 1997 as part of their PhD studies and stored at the Australian National University. The present study uses samples from all stages of mineralisation from unaltered precursor black shales to high grade Stage II material from the ANU suite.

Representative samples from each generation of mineralisation as well as precursor black shales were selected. Sections of 32 samples were cut and set in round 20 mm diameter epoxy resin mounts. Mounts were trimmed to a thickness of ~ 5 mm and polished. Initial stages of polishing were conducted by hand sanding (to remove coarse surface and expose sample), with subsequent polishing for 20 minutes on 8 µm, 3 µm then 1 µm, automated diamond paste polishing pads.

Etching

Polished mounts were etched to expose growth zones in pyrites. A concentrated sodium hypochlorite (NaOCl) solution was applied to the surface of each polished section for 1-2 minutes (after Cox et al., 1981) before mounts were rinsed with water and dried. Samples were then examined under reflected light and a refined selection of individual pyrites from each generation was identified for further analysis.

Final Mounts

In order to reduce the number of mounts for S isotope analyses and to incorporate standards required for in situ sulfur isotope analyses, selected pyrites were cut from original polished mounts and re-mounted into three 2 cm epoxy mounts. These mounts were polished and prepared as previously described and re-etched to locate, photograph and characterise pyrites of interest. The etch was removed prior to analysis by polishing on a 1 µm diamond paste polishing pad for 2-5 minutes. Pyrites were subsequently photographed in reflected light.

Final mounts incorporate 21 samples from across the paragenetic suite including unaltered host black shales, Pre-Stage I (G veins), Stage I (A veins), Stage I/II vein intersections and SII (D veins).

Electron Microprobe Analysis

Major element and select trace element compositions were determined by Electron Microprobe Analysis (EMPA) using a Cameca SX100 at the Research School of Earth Sciences, ANU. Elements and X-ray lines used for analyses were – Fe (K_α), S (K_α), Cu (K_α), Ag (L_α), As (K_α) Au (M_α) and Sb (L_α). Operating conditions for quantitative spot analyses consisted of an accelerating voltage of 15 kV, a beam current of 100 nA and a focused electron beam (~1 µm in diameter) with wavelength dispersive X-ray spectrometers. To optimise count rates of individual elements, counting times were set as: Fe – 10 s, S – 10 s, Ag – 60 s, As – 30 s, Au – 30 s, Cu – 60 s and Sb – 60 s. Standards used for calibration were troilite (Fe: 63.5%, S: 36.5%) for Fe and S, and elemental ingots for As, Au, Ag, Sb and Cu. Analyses took place in a single 24 hour session. In total 183 spot analyses were conducted (including standards and non-pyrite phases) across 9 samples in order to characterise the major element composition of pyrites across all stages of mineralisation.

Two dimensional element maps were obtained for Fe, S, Cu, As and Au, under operating conditions of accelerating voltage of 15 kV; beam current of 200 nA; grid spacing ~1 µm and counting time of 200 milliseconds. The electron microprobe (EMP) was run in mapping mode allowing automated analysis overnight. A total of four grains were mapped over a period of 4-5 hours each. Maps depict relative abundances of elements of interest, allowing the determination of compositional zones. In order to quantify relative variations observed in element maps, core to rim spot traverses with a 3 µm step size were undertaken after grains were mapped. Elements collected during traverses were Fe, S, Cu, Ag, Au, As and Sb under the same conditions outlined for spots above.

In order to reduce error on measurements, spots and traverses were individually programed and carefully positioned on clean flat sections of pyrite away from grain boundaries, cracks or inclusions. Standard – sample bracketing allowed for correction of instrument drift. Data appear normally distributed about 100, with weight % totals between 98 and 102 considered viable, and data falling outside this range disregarded. Detection limits and standard deviations for each measurement were obtained during data reduction and taken into account during data interpretation.

Sensitive High Resolution Ion Microprobe – Stable Isotopes

Sulfur isotope analyses were conducted using the Sensitive High Resolution Ion Microprobe for Stable Isotopes (SHRIMP-SI) at the Research School of Earth Sciences, ANU. The SHRIMP-SI is designed to conduct in situ, high resolution, measurements of stable isotopes with a low mass range – capable of precise concurrent measurements of ^{32}S, ^{33}S, ^{34}S and ^{36}S. The instrument utilises the principles of secondary ion mass spectrometry with a detailed description of systematics outlined in Ireland et al. (2008).

Ultimately, 68 pyrites from 18 samples across three polished mounts were analysed for ^{32}S, ^{33}S and ^{34}S over two sessions, one session of 24 hours (one mount) duration and a second of 48 hours (two mounts). ^{36}S was excluded as its low abundance drastically increases acquisition time – from ~ 6 minutes per spot to ~ 30 minutes per spot (in order to obtain reasonable counting statistics) and preliminary data plotted within error of the mass dependent fractionation line.
Operating conditions were held constant between sessions and are summarised in Table 1.

Table DR1: Summary of operating conditions for SHRIMP - SI sulfur isotope analyses.

Spot Size	27 µm
Isotopes collected	^{32}S, ^{33}S and ^{34}S
Primary Beam	7 nA
Secondary beam	5 x 10^8 cps
Raster (to establish baseline)	2 minutes
Data Acquisition	10 individual integrations of 10 seconds

A spatial resolution of approximately 30 µm was attained and where grain size was sufficient, multiple analyses were undertaken to target different growth zones previously identified. Sample measurements were bracketed every 4-5 analyses by at least one standard measurement to ensure precision and account for instrument drift.

Data were reduced by Dr. Peter Holden at the Research School of Earth Sciences, ANU using Ruttan pyrite from Manitoba, Canada with an accepted standard $\delta^{34}S$ value of 1.2‰ (Crowe

and Vaughan, 1996). Sulfur isotope data are reported as $\delta^{34}S$, which is defined relative to Vienna Canyon Diablo Troilite (V-CDT) as:

$$\delta^{34}S = \left(\frac{\left(\frac{^{34}S}{^{32}S}\right)_{sample} - \left(\frac{^{34}S}{^{32}S}\right)_{V-CDT}}{\left(\frac{^{34}S}{^{32}S}\right)_{V-CDT}} \right) \cdot 10^3 \qquad \textit{Eqn. 2.1}$$

(Faure, 1986)

Error to two standard deviations was calculated for each session and mount analysed, error averaging ~0.5 per mil (Table 2).

Table DR2: Reproducibility of sulfur isotope ratios in Ruttan pyrite (standard $\delta^{34}S$ = 1.2‰).

Mount	Session	Standard Reproducibility (2σ)	
		$\delta^{33}S$ (‰)	$\delta^{34}S$ (‰)
I	1	0.62 ± 0.53	1.2 ± 0.68
II	2	0.62 ± 0.47	1.2 ± 0.37
III	2	0.63 ± 0.50	1.2 ± 0.53

A plot of $\delta^{33}S$ vs. $\delta^{34}S$ shows sulfur isotope data plot on the mass dependent fractionation line ($\delta^{33}S/\delta^{34}S$ = 0.515) attesting to the accuracy of analyses and indicating fractionation observed in S isotopes is attributable to mass-dependent processes.

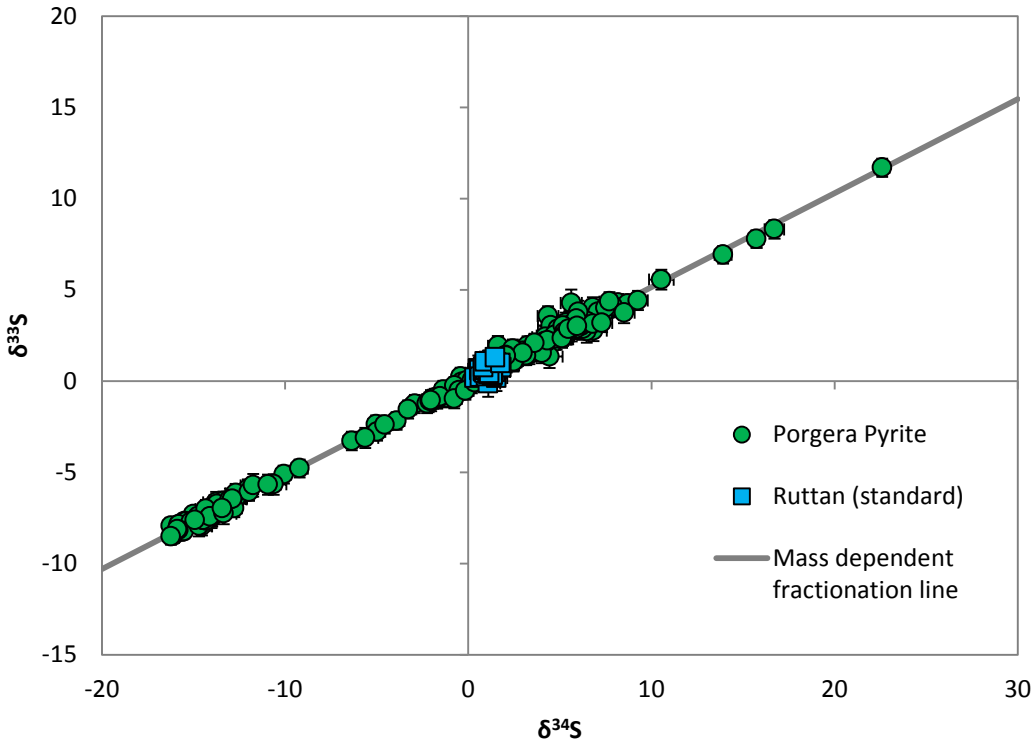

Fractionation line $\delta^{33}S$ vs. $\delta^{34}S$ indicating analyses are consistent with mass dependent fractionation.

To determine if the etching of samples had any significant effect on sulfur isotope composition, two standard pyrite grains of known composition (Ruttan: $\delta^{34}S$ = 1.2‰) were analysed un-etched to establish any baseline variation between grains. One grain was subsequently etched, whilst the other grain remained untreated and the mount was repolished (as all samples were). Both grains were then re-analysed. No significant effect was observed.

Finally, an image of each spot was taken at the time of analysis and data associated with spots that appear out of focus or on major cracks or incorporating phases other than pyrite are disregarded. SHRIMP measurements were undertaken prior to LA-ICP-MS analyses to minimise surface disturbance and ensure only undamaged, pristine surfaces were analysed.

Laser Ablation Inductively Coupled Plasma Mass Spectrometry

Laser Ablation Inductively Coupled Plasma Mass Spectrometry (LA-ICP-MS) was used to accurately measure the concentration of trace elements and identify compositional heterogeneity within individual pyrite grains. A fundamental advantage of using LA-ICP-MS is the 'time-slice' nature of data acquisition – which allows the in situ identification of mineral inclusions and compositional zoning within a single grain (Longerich et al., 1996). In the case of mineral traverses, 'time-slice' data may be calibrated to stage movement and lengths of traverses delineated.

LA-ICP-MS for this study was undertaken at the Research School of Earth Sciences, ANU. The sample was ablated and collected using a Lambda Physik laser ablation system that operates at a wavelength of 193 nm. Operating conditions consisted of a laser output energy of 45mJ (±2 mJ) with a repetition rate of 5 Hz. The ablated sample was transported in a mixture of H-He-Ar through a cross-flow nebuliser to an Agilent Technologies 7700 series quadrupole ICP-MS which yields detection limits of ~0.01 ppm for most elements. Isotopes of each element to be analysed, length of analysis (for spots) and dwell time were set to minimise potential interferences and maximise counting statistics – with overall mass sweep time kept to ~1 s. Elements predicted to have lower concentrations were assigned slightly longer dwell times where appropriate. Data reduction was undertaken using Iolite software (Paton et al., 2011) in accordance with standard methods (Longerich et al., 1996). Limits of

detection (LOD) are individually assigned to each element and vary between analyses. The calculations controlling LOD are examined in detail in Longerich et al. (1996).

Pyrites from each generation were analysed using LA-ICP-MS. Analyses took place over two 18 hour sessions. Spatial resolution and grain size dictated two methods for trace element analyses. In the majority of analyses, where grain size was sufficient, mineral traverses across growth zones were undertaken. This was the preferred method as much of the compositional zoning identified was extremely fine and traverses have provide greater spatial resolution than spots. Where grain size was small (< 50 µm) spot analyses were used.

NIST-610 and Mass 1 (PS-1) were used as standards to calibrate trace element concentrations. Both standards were compared with published values to confirm homogeneity of standards with respect to elements of interest and proved to be well within error (Appendix 2.2). Standards were analysed regularly to bracket sample measurements, with additional standards run at the commencement and conclusion of each session and either side of any significant break in data acquisition. Data were reduced relative to both NIST-610 and Mass-1 (PS-1) standards in order to determine differences that may arise between silicate glass and Fe-sulfide standard materials. Comparison of reduced data yielded no significant difference in element concentrations. Consequently, NIST-610 was deemed the most appropriate standard incorporating the greatest number of target elements and appeared more homogenous during data acquisition. Stoichiometric Fe (46.55 wt %) was used as an internal standard as a means of correcting for multiple sources of error such as matrix effects and sensitivity drift (Longerich et al., 1996).

Spot Analyses

Pyrite spot analyses were conducted in the second session using a laser spot size of 28 µm. A total of 33 spot analyses were conducted across pyrites from four separate samples. Samples were run in batches of 11 spots, bracketed by two NIST-610 and one Mass-1 (PS-1) standard analyses. Each analysis ran for 70 s – 30 s measuring background (laser off) and 40 s analysis (laser on). Elements collected are the same as for mineral traverses in session 2 (Table 3).

Mineral Traverses

Traverses were conducted across two sessions using a slit to focus the laser beam. Operating conditions were adjusted slightly after the first session to refine and optimise results (Table 3).

Table DR3: Operating conditions for LA-ICP-MS mineral traverses.

	Session One	Session Two
Repetition rate (Hz)	5	5
Pre ablation (background)	30 s	30 s
Analyses per batch	5	6
Slit width (µm)	~ 6 µm	~ 6 µm
Slit length (µm)	~ 70 µm	~ 35 µm
Elements collected	^{29}Si, ^{34}S, ^{51}V, ^{43}Ca, ^{52}Cr, ^{57}Fe, ^{59}Co, ^{60}Ni, ^{63}Cu, ^{66}Zn, ^{75}As, ^{77}Se, ^{82}Se, ^{95}Mo, ^{107}Ag, ^{118}Sn, ^{121}Sb, ^{125}Te, ^{181}Ta, ^{182}W, ^{195}Pt, ^{197}Au, ^{208}Pb and ^{209}Bi	^{51}V, ^{52}Cr, ^{57}Fe, ^{55}Mn, ^{59}Co, ^{60}Ni, ^{63}Cu, ^{66}Zn, ^{75}As, ^{77}Se, ^{95}Mo, ^{107}Ag, ^{118}Sn, ^{121}Sb, ^{125}Te, ^{181}Ta, ^{182}W, ^{195}Pt, ^{197}Au, ^{208}Pb and ^{209}Bi
Scan speed (µm/s)	2	2

Scans were performed by manually aligning the long axis of the slit parallel to the grain boundary and programming a perpendicular transect from the grain boundary to a desired end point. The length of each traverse varied between grains but all analyses were aimed at targeting core to rim compositional heterogeneities.

Each batch of traverses was bracketed on each side by one NIST-610 and one Mass 1 (PS-1) standard measurement. Each scan was repeated to minimize uncertainty and to ensure samples were not contaminated with remnant gold coating from SHRIMP-SI analysis.

Log-Liner sulfur isotope vs trace element plots

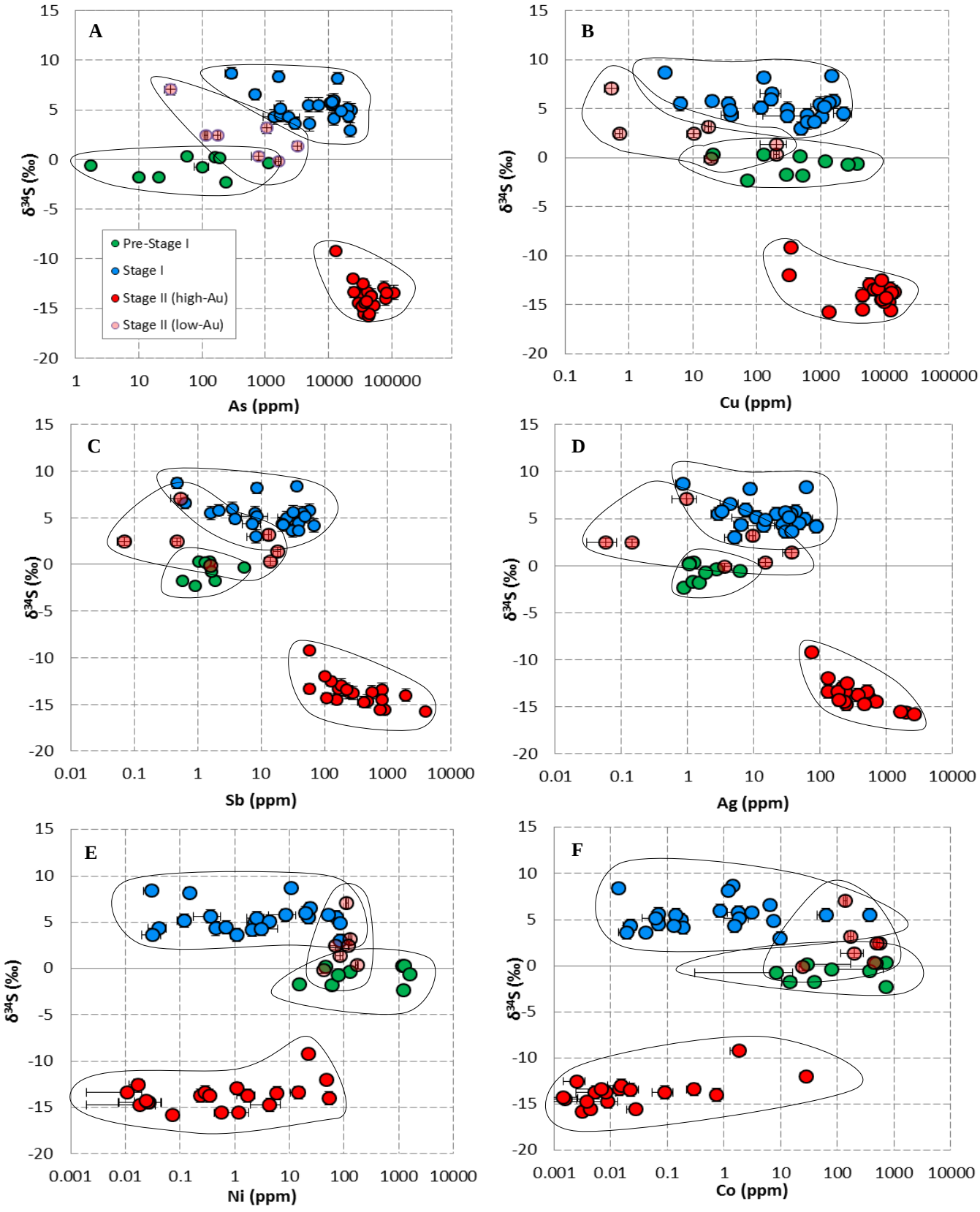

Log-linear plot of $\delta^{34}S$ (‰) vs (A) As (ppm), (B) Cu (ppm), (C) Sb (ppm), (D) Ag (ppm), (E) Ni (ppm) and (F) Co (ppm).

Table DR4: SHRIMP-SI sulfur isotope measurements from samples across the Porgera paragenetic sequence. All data are from pyrite crystals within veins, with the exception of black shale where pyrites occurred disseminated throughout.

Stage	$\delta^{33}S$ (‰)	2 standard error	$\delta^{34}S$ (‰)	2 standard error
Black Shale	1.07	0.50	2.36	0.43
Black Shale	1.71	0.47	3.46	0.43
Black Shale	1.94	0.51	3.23	0.46
Black Shale	1.63	0.52	3.46	0.45
Black Shale	3.34	0.49	6.97	0.38
Black Shale	1.38	0.50	3.01	0.42
Black Shale	11.69	0.50	22.60	0.40
Black Shale	6.92	0.49	13.91	0.47
Black Shale	3.05	0.48	5.47	0.43
Black Shale	8.31	0.52	16.72	0.53
Black Shale	4.13	0.47	8.02	0.40
Black Shale	4.28	0.49	8.18	0.43
Black Shale	2.00	0.50	4.54	0.46
Black Shale	7.77	0.49	15.74	0.38
Black Shale	-1.26	0.50	-2.91	0.47
Black Shale	-0.94	0.51	-1.19	0.43
Black Shale	-1.23	0.48	-2.17	0.42
Black Shale	-1.24	0.52	-2.25	0.44
Black Shale	-0.99	0.52	-1.93	0.42
Black Shale	-0.57	0.49	-0.68	0.40
Black Shale	-2.38	0.50	-5.03	0.44
Black Shale	-0.64	0.48	-0.87	0.44
Black Shale	-3.29	0.51	-6.36	0.45
Black Shale	-2.19	0.49	-3.92	0.42
Black Shale	-2.78	0.49	-4.99	0.44
Black Shale	-2.40	0.48	-4.56	0.44
Black Shale	0.24	0.50	-0.42	0.42
Black Shale	-0.98	0.54	-1.70	0.49
Black Shale	0.13	0.51	0.38	0.46
Black Shale	-0.48	0.50	-1.36	0.44
Pre SI	-1.55	0.50	-3.29	0.44
Pre SI	-1.10	0.48	-2.10	0.39
Pre SI	-0.88	0.49	-1.52	0.49
Pre SI	-0.37	0.49	-0.41	0.44
Pre SI	0.47	0.49	1.03	0.43
Pre SI	0.23	0.49	0.28	0.45
Pre SI	-0.91	0.49	-1.74	0.42
Pre SI	-0.92	0.50	-1.83	0.43
Pre SI	-0.19	0.48	0.18	0.44
Pre SI	-0.06	0.50	-0.37	0.43
Pre SI	0.03	0.49	-0.08	0.43
Pre SI	3.76	0.47	7.28	0.45
Pre SI	1.18	0.49	1.93	0.41
Pre SI	3.71	0.49	7.81	0.44
Pre SI	-0.45	0.48	-0.59	0.43
Pre SI	-0.25	0.48	-0.74	0.45
SI	4.24	0.52	8.70	0.54
SI	2.94	0.52	6.56	0.57
SI	1.94	0.53	1.62	0.54
SI	3.57	0.54	4.35	0.58
SI	4.27	0.75	5.62	0.57
SI	2.80	0.56	4.12	0.72
SI	3.08	0.60	4.44	0.71
SI	3.46	0.57	5.73	0.71
SI	3.75	0.56	6.17	0.71
SI	1.92	0.62	4.43	0.72
SI	3.63	0.56	4.52	0.72
SI	2.99	0.58	4.21	0.72
SI	2.72	0.56	4.31	0.74
SI	3.60	0.58	5.47	0.72
SI	3.42	0.61	5.50	0.70
SI	3.34	0.59	5.49	0.71
SI	2.90	0.60	4.83	0.71
SI	3.34	0.58	6.84	0.72
SI	3.90	0.59	5.76	0.71
SI	2.55	0.59	3.61	0.71
SI	3.24	0.61	5.11	0.71
SI	3.55	0.58	5.50	0.72
SI	3.82	0.59	5.50	0.73
SI	3.74	0.54	5.82	0.71
SI	3.66	0.60	6.24	0.71
SI	3.31	0.63	6.46	0.71
SI	3.77	0.56	5.32	0.72
SI	3.40	0.64	5.65	0.71
SI	3.85	0.57	6.31	0.71

SI	3.58	0.66	5.71	0.70
SI	3.72	0.55	6.29	0.71
SI	4.14	0.62	6.51	0.71
SI	3.67	0.59	6.40	0.71
SI	4.67	0.59	7.79	0.71
SI	3.82	0.56	5.95	0.72
SI	3.21	0.59	5.04	0.71
SI	3.92	0.60	6.43	0.71
SI	3.70	0.56	6.44	0.72
SI	3.87	0.56	6.50	0.72
SI	3.44	0.60	6.25	0.71
SI	3.79	0.54	6.53	0.71
SI	3.86	0.56	6.42	0.71
SI	3.87	0.55	6.61	0.73
SI	4.31	0.58	7.42	0.70
SI	3.79	0.55	6.49	0.70
SI	4.60	0.57	6.80	0.71
SI	4.68	0.57	7.89	0.72
SI	3.70	0.55	6.19	0.71
SI	3.73	0.62	6.15	0.71
SI	3.73	0.59	6.16	0.70
SI	3.56	0.54	5.41	0.70
SI	3.23	0.64	5.45	0.71
SI	3.82	0.58	6.57	0.69
SI	3.59	0.56	6.17	0.71
SI	3.82	0.55	6.39	0.70
SI	3.83	0.57	6.45	0.70
SI	3.91	0.54	6.41	0.71
SI	3.92	0.58	6.61	0.70
SI	3.90	0.60	6.62	0.71
SI	3.96	0.57	6.81	0.71
SI	4.36	0.55	7.08	0.71
SI	3.69	0.58	5.80	0.70
SI	3.85	0.57	6.49	0.71
SI	3.45	0.56	5.91	0.72
SI	3.66	0.58	6.03	0.72
SI	3.21	0.59	4.97	0.70
SI	2.75	0.55	4.17	0.72
SI	2.11	0.56	4.01	0.70
SI	3.44	0.56	4.89	0.71
SI	1.35	0.65	1.20	0.73
SI	3.63	0.58	5.51	0.69
SI	4.36	0.63	6.01	0.72
SI	3.10	0.58	4.72	0.71
SI	0.51	0.64	1.74	0.53
SI	4.42	0.53	9.26	0.53
SI	5.55	0.54	10.54	0.68
SI	4.01	0.54	7.51	0.53
SI	4.36	0.51	7.71	0.55
SI	3.75	0.58	8.50	0.57
SI	2.81	0.51	5.56	0.58
SI	3.11	0.52	6.15	0.58
SI	3.40	0.52	5.91	0.59
SI	2.87	0.53	5.55	0.56
SI	3.01	0.53	5.17	0.56
SI	2.67	0.52	5.24	0.57
SI	2.21	0.53	4.32	0.56
SI	2.45	0.53	5.17	0.56
SI	2.34	0.52	5.11	0.57
SII	-6.35	0.57	-13.77	0.70
SII	-6.36	0.58	-13.40	0.69
SII	-6.92	0.56	-14.01	0.71
SII	-6.22	0.56	-13.56	0.71
SII	-6.30	0.62	-13.86	0.71
SII	-6.80	0.58	-13.99	0.71
SII	-6.06	0.58	-13.76	0.71
SII	-6.31	0.57	-13.36	0.71
SII	-6.29	0.57	-13.71	0.72
SII	-7.37	0.56	-14.71	0.72
SII	-5.93	0.54	-12.03	0.56
SII	-6.44	0.51	-12.64	0.56
SII	-6.45	0.52	-12.70	0.58
SII	-6.16	0.53	-12.70	0.55
SII	-7.67	0.53	-14.31	0.57
SII	-7.62	0.51	-14.51	0.55
SII	-7.50	0.51	-14.30	0.56
SII	-6.59	0.53	-13.36	0.55
SII	-6.94	0.51	-13.76	0.54
SII	-7.40	0.53	-14.47	0.58
SII	-7.42	0.52	-14.74	0.57
SII	-7.62	0.53	-14.47	0.56

SII	-6.75	0.51	-13.72	0.56
SII	-7.01	0.51	-14.33	0.57
SII	-7.43	0.52	-14.11	0.53
SII	-7.63	0.52	-14.92	0.57
SII	3.12	0.50	6.81	0.56
SII	3.18	0.50	7.30	0.56
SII	1.39	0.51	3.17	0.57
SII	-0.53	0.49	-0.50	0.41
SII	1.37	0.50	2.52	0.42
SII	1.02	0.49	2.46	0.44
SII	1.08	0.51	2.31	0.43
SII	0.04	0.49	0.20	0.41
SII	-0.86	0.49	-1.54	0.44
SII	1.77	0.51	2.43	0.44
SII	1.03	0.52	1.74	0.44
SII	0.78	0.52	0.74	0.45
SII	0.62	0.51	0.96	0.43
SII	0.98	0.54	1.88	0.45
SII	-0.98	0.51	-0.77	0.42
SII	0.39	0.51	1.52	0.43
SII	-0.54	0.48	-0.15	0.44
SII	1.40	0.50	2.05	0.44
SII	1.07	0.50	2.49	0.43
SII	2.08	0.51	3.63	0.52
SII	-5.12	0.49	-10.07	0.38
SII	2.84	0.52	5.47	0.44
SII	-6.98	0.48	-12.77	0.42
SII	-0.07	0.50	0.34	0.45
SII	-6.08	0.49	-11.98	0.43
SII	0.64	0.47	1.36	0.48
SII	-4.79	0.50	-9.21	0.45
SII	-5.08	0.56	-10.62	0.69
SII	0.87	0.57	0.87	0.72
SII	2.11	0.57	2.97	0.71
SII	1.37	0.55	1.54	0.70
SII	1.95	0.60	2.06	0.69
SII	3.58	0.65	5.94	0.73
SII	-0.49	0.57	-2.04	0.72
SII	1.51	0.59	1.65	0.71
SII	-5.13	0.63	-11.74	0.70
SII	-6.68	0.59	-13.35	0.70
SII	-5.09	0.55	-10.94	0.69
SII	-5.92	0.61	-13.02	0.70
SII	-5.88	0.55	-12.89	0.71
SII	-6.40	0.57	-13.43	0.72
SII	1.61	0.56	1.73	0.71
SII	-7.31	0.38	-15.00	0.26
SII	-8.12	0.38	-15.91	0.20
SII	-8.24	0.40	-15.88	0.22
SII	-8.12	0.37	-15.66	0.23
SII	-8.00	0.39	-15.77	0.22
SII	-7.93	0.43	-16.24	0.24
SII	-8.49	0.36	-16.07	0.24
SII	-8.04	0.38	-15.84	0.22
SII	-8.06	0.40	-15.43	0.21
SII	-7.83	0.39	-15.41	0.23
SII	-8.09	0.39	-15.82	0.22
SII	-7.80	0.39	-14.97	0.26
SII	-8.27	0.39	-15.59	0.18
SII	-7.70	0.41	-15.50	0.20
SII	-7.86	0.37	-15.78	0.20
SII	-7.92	0.38	-15.32	0.27
SII	-7.71	0.39	-15.44	0.23
SII	-7.87	0.39	-15.80	0.21
SII	-7.70	0.40	-15.14	0.24
SII	-8.24	0.38	-15.51	0.24
SII	-8.18	0.40	-15.81	0.21
SII	-8.14	0.37	-15.88	0.29
SII	-8.52	0.45	-16.24	0.25

REFERNCES CITED

Cox, S.F., Etheridge, M.A. & Hobbs, B.E., 1981, The experimental ductile deformation of polycrystalline and single crystal pyrite, *Economic Geology*, 76:2105-2117.

Crowe, D.E. and Vaughan, R.G., 1996, Characterisation and use of isotopically homogenous standards for in situ laser microprobe analyses of 34S/32S ratios, *American Mineralogist*, 81:187-93.

Faure, G., 1986, Principles of Isotope Geology, New York, John Wiley & Sons.

Ireland, T.R., Clement, S., Compston, W., Foster, J.J., Holden, P., Jenkins, B., Lane, P., Schram, N. & Williams, I.S., 2008, Development of SHRIMP, *Australian Journal of Earth Sciences*, 55(6-7):937-54.

Longerich, H.P., Jackson, S.E. & Gunther, D., 1996, Laser ablation inductively coupled mass spectrometric transient signal data acquisition and analyte concentration calculation, *Journal of Analytical Atomic Spectroscopy*, 11: 899-904.